Coronal Hard X-ray Emission Associated with Radio Type III Bursts

Säm Krucker[1], P. Saint-Hilaire[1], S. Christe[1,2], S.M. White[3], A.D. Chavier[4], S.D. Bale[1,2], & R. P. Lin[1,2]

krucker@ssl.berkeley.edu

ABSTRACT

We report on a purely coronal hard X-ray source detected in a partially disk-occulted solar flare by the Reuven Ramaty High Energy Solar Spectroscopic Imager (RHESSI) that is associated with radio type III bursts and a suprathermal electron event detected near 1 AU by the WIND 3-D Plasma & Energetic Particle (3DP) instrument. Several observational characteristics suggest that the coronal hard X-ray source is thin target bremsstrahlung emission from the escaping electrons that produce the radio type III bursts. The hard X-ray emission correlates in time with the radio type III bursts and originates from a radially elongated source in the corona with a length ($\sim$65 Mm) similar to typical coronal density scale heights. Furthermore, the difference between the hard X-ray photon spectral index (γ=4.1$\pm$0.4) and the electron spectral index of the in-situ observed event ($\delta_{in-situ}$=2.9$\pm$0.3) is around 1, consistent with the thin target interpretation. A futher test for the thin target scenario is to compare the number of electrons needed to produce the observed hard X-ray emission with the number of in-situ observed electrons. However, the number of escaping electrons derived from the single-spacecraft WIND measurement is in the best case an order of magnitude estimate and could easily underestimate the actual number of escaping electrons. Using the WIND observations, the estimated number of escaping electrons is about an order of magnitude too low. Thus, the thin target interpretation only holds if the WIND measurements are significantly underestimating the actual number of escaping electrons. Future multi-spacecraft observations with STEREO, SOLAR ORBITER, and SENTINELS will resolve this uncertainty.

[1]Space Sciences Laboratory, University of California, Berkeley, CA 94720-7450, USA

[2]Department of Physics, University of California, Berkeley, CA 94720-7300, USA

[3]Department of Astronomy, University of Maryland, College Park, MD 20742, USA

[4]Chavier Caamaño, ¡Si Si!, Berkeley, CA 94705, USA

Subject headings: Sun: flares — Sun: particle emission — Sun: X-rays, gamma rays

1. Introduction

Acceleration of suprathermal (>1 keV) electrons on the Sun occur frequently in solar flares (e.g. review by Hudson et al. 2004) and Coronal Mass Ejections (e.g. review Hudson et al. 2006), and also during many different kinds of burst seen in radio observations (Bastian, Benz, & Gary 1998). Several different acceleration mechanisms are proposed to explain suprathermal electrons, however, currently it is not understood how electrons are accelerated. Suprathermal electrons on closed magnetic field lines (i.e. both ends are connected to the Sun) eventually lose their energy and are thermalized. Collisions with the ambient plasma is a loss mechanism that is always present producing hard X-ray emission by the bremsstrahlung mechanism. Since the intensity of bremsstrahlung emissions is proportional to the ambient plasma density, hard X-ray emission is generally most prominent from chromospheric footpoints of flare loops, but much fainter coronal emissions are also present (e.g. Frost & Dennis 1971, Hudson 1978, Kane et al. 1992, Masuda 1994, Tomczak 2001, Sui et al. 2003, Somov et al. 2004, Battaglia & Benz 2006, Krucker et al. 2007c, Krucker & Lin 2008, Krucker et al. 2008). Electrons with access to magnetic field lines that are open to interplanetary space, however, can escape from the Sun, as the coronal column densities are generally too low to stop suprathermal (>10 keV) electrons. Hard X-ray bremsstrahlung emissions are also produced in this scenario, although at a much lower intensity than in chromospheric footpoints in the thin target approximation (e.g. Brown 1971). This emission is expected to trace the path of the escaping electrons and it is expected to have an elongated source shape with a FWHM length roughly equal to the density scale height in the corona (typically of the order of $\sim 10^{10}$ cm). However, thin target emissions of escaping electrons have not been positively identified.

There are two well established methods of observing escaping electron beams. Firstly, radio observations in the decimeter and longer wavelength ranges show emissions that drift rapidly from high to low frequencies as a function of time (so called radio type III bursts, for a review, see Reiner 2001). Escaping electron beams are generally unstable to the bump-on-tail plasma instability and produce Langmuir plasma waves, that then interact with density fluctuations and other waves to generate radio waves at about the local plasma frequency. The frequency drift is produced as the unstable part of the electron beam moves away from the Sun from higher to lower densities resulting in emissions at progressively lower plasma frequencies. Secondly, escaping electron beams can be directly measured by in-situ particle

detectors (e.g. review by Lin 1985) providing measurements of electron spectra and rough estimates of the total number of escaping electron beams. Some of the in-situ observed electron beams are temporally and spectrally related to solar flare hard X-ray emissions (Dröge 1995, Krucker et al. 2007a) and are therefore called prompt events, while other events are clearly delayed relative to the flare hard X-ray emissions and are speculated to be accelerated by coronal shocks (Krucker et al. 1999, Haggerty & Roelof 2002). The temporal and spectral correlation for prompt events suggests a common acceleration mechanism for the hard X-ray producing electrons and the escaping electrons. However, the observed number of escaping electrons is typically only a fraction of a percent compared to the number of electrons in the flare (e.g. Lin & Hudson 1971). Therefore, the expected thin target hard X-ray emission of escaping electron beams is roughly three to four orders of magnitude smaller than the thick target hard X-ray emission from downward moving electrons in the flare (e.g. Saint-Hilaire et al. 2008). Present-day hard X-ray imagers do not provide a large enough dynamic range to observe this. For totally disk-occulted flares, however, the sensitivity of the Reuven Ramaty High Energy Solar Spectroscopic Imager (RHESSI, Lin et al. 2002) should be high enough to detect emissions from escaping electron beams, at least under favorable conditions (Saint-Hilaire et al. 2008). In this paper, we report the first detection and imaging of hard X-ray emissions temporally correlated with suprathermal electrons that produce radio type III bursts as they escape into interplanetary space.

2. Observations and data analysis

In November 2006, AR10923 produced more than 200 flares mostly below GOES C-class, but with unusually intense hard X-ray emissions compared to their thermal soft X-ray flux (Krucker et al. 2007b, Hannah et al. 2008, Nitta et al. 2008). After AR10923 reached longitudes past W20, at least 18 solar impulsive electron events were detected near Earth by the 3-D Plasma & Energetic Particle (3DP) instrument (Lin et al. 1995) onboard the WIND spacecraft. The last electron event is recorded on November 21 around 19:50 UT (Figure 1, right) when AR10923 was already clearly behind the solar limb. Extrapolating flare locations from times when AR10923 was visible on the disk to the time of the last electron event indicate that the flare occurred $12.5\pm2.3^\circ$ behind the solar limb, corresponding to an occultation height of about $24''$ ($\sim$17 Mm). The electron event is clearly seen down to 6 keV, but not below. The observed onset of the electron event seen near 1 AU is impulsive and shows clear velocity dispersion (Figure 1, right), suggesting that the event is magnetically well connected to the flare site. This is rather unusual for a flare site 12° behind the solar limb, as the nominal Parker spiral for this event would connect to W66. However, differences between the nominal Parker spiral footpoint and the actual flare site of up to 90° have been

reported (e.g. Wibberenz & Cane 2006, Klein et al. 2008).

Interplanetary radio observations by the WAVES instruments onboard the WIND and STEREO spacecraft (Bougeret et al. 1994, Bougeret et al. 2008) show a single type III radio burst (Figure 1, right) that correlates in time with the derived solar release (19:27±00:03 UT) of the energetic electrons seen near 1 AU (for discussion on derivation and systematic errors of onset times see Krucker et al. 1999, Lintunen & Vainio 2004, and Saiz et al. 2005). The most intense in-situ Langmuir waves are seen between 20:06 and 20:35 UT (Figure 1, right, third panel from top) when 4-10 keV electrons start to arrive at WIND indicating that electrons at these energies produce the interplanetary radio type III burst. In the meter range, the Green Bank Solar Radio Burst Spectrometer (GBSRBS) reveals that there are two type III bursts that merge into a single burst in the interplanetary observations (Figure 1, left). The radio emission starts at ∼50 MHz corresponding to a plasma density of $3{\cdot}10^7$ cm^{-3}. This is a rather low density for an occultation height of only 17 Mm, suggesting either that the radio emission is not coming from just above the (projected) limb but rather from higher in the corona, or else it comes from unusually low density coronal field lines. At lower altitudes, the wave growth might be damped, or the radio emission is not able to escape in the direction to Earth. In either case, the derived value of $3{\cdot}10^7$ cm^{-3} gives a lower limit to the density along the escape path visible from Earth.

2.1. X-ray time profiles and imaging

The thermal flare emission associated with the interplanetary electron event is difficult to see in the GOES time profiles, but RHESSI observes a clear increase in the 4-8 keV emission. Before the type III bursts, a decaying hard X-ray source from the western limb (972″; 52″) is seen (Figure 2, left, and magenta curve in Figure 1), while at the onset of the first type III burst a second source at the western limb appears (Figure 2, middle, and red curve in Figure 1) that is about 55″ south of the decaying source. Both sources are partially disk-occulted and elongated along the limb by 10″. At the peak of the thermal emission, the density derived from the observed RHESSI emission measure ($4{\cdot}10^{45}$ cm^{-3}) and volume is of the order of $8{\cdot}10^9$ cm^{-3}. At the time of the type III bursts, the emission measure is difficult to derive, but it is smaller by about an order of magnitude implying a density that is about three times lower than during the peak.

Above 14 keV, RHESSI observes a second component which shows initially two peaks that have the same onset times as the two type III bursts seen at meter wavelengths, but the FWHM duration in hard X-rays is about three times longer than the type III burst duration at a given frequency. The 14-30 keV emission observed after the type III bursts around 19:25

UT is interpreted as a thermal emission because it is co-spatial with the 4-8 keV thermal emission (Figure 2, right) and has a very soft spectra ($\gamma \sim 8$). The two hard X-ray peaks correlated with the type III bursts are very weak, and can only be imaged with a reduced spatial resolution of 60″ using RHESSI detectors 7 through 9 (Hurford et al. 2002). The 14-30 keV image shows a different source centroid than the thermal emission with a coronal location at an altitude of ∼50″ above the limb (Figure 2, middle). Furthermore, the source is extended in the radial direction with a FWHM length of ∼90″ (∼ 65 Mm) and is unresolved in the direction along the limb. The derived length is of the same order as typical coronal density scale heights, and corresponds to a temperature of ∼1.3 MK in the barometric model, i.e., the hard X-ray images looks much as we would expect hard X-rays from a Type III burst to look.

Around the time of the type III radio burst, the X-ray Telescope (XRT, Golub et al. 2007) onboard the Hinode mission (Kosugi et al. 2007) was observing with two filters ('Al-poly' and 'medium Be') with a five minute cadence. Figure 3 shows the 'medium Be' images before and after the type III bursts including the difference image. The two hard X-ray sources seen by RHESSI are also detected in the XRT images, but they are saturated making further analysis difficult. In the difference image, weakly enhanced emissions are observed from in-between the two sources. The relation of this weak brightening with the escaping electrons is unclear. Contrary to many other X-ray events related to impulsive electron events (e.g. Aurass et al. 1994, Wang et al. 2005, Pick et al. 2005), no X-ray jet is observed (Nitta et al. 2008). However, a possible X-ray jet could have been missed because of the 5 minute cadence.

2.2. Spectral analysis

The cumulative radiation damage of the RHESSI detectors makes spectral fitting below 10 keV difficult (see Hannah et al. 2008 for details). However, here we are mostly interested in the spectrum of the elongated coronal source above 14 keV. The observed spectrum can be fitted with a power law with a slope of γ=4.1±0.4 (Figure 4, left). In the thin target approximation (e.g. Brown 1971), the hard X-ray producing electron beam would have a spectral slope of δ_{hxr}=3.1±0.4. This is similar to the spectrum of the in-situ observed electrons that when fitted over energies above 20 keV gives $\delta_{in-situ}$=2.9±0.3, or, if fitted with a broken power law fit, gives values of $\delta_{in-situ}$=2.5±0.4 below ∼90 keV (Figure 4, right).

The instantaneous number of electrons needed to produce the observed hard X-ray emission in the thin target approximation is straight-forward to derive, but depends on the

ambient plasma density in the hard X-ray source. The start frequency of the radio type III burst gives a lower limit for the ambient density as mentioned above. An upper limit for the ambient density can be derived from the maximal column density that allows electrons to escape (e.g. Emslie 1978). For 20 keV electrons, the column density has to be lower than $\sim 6{\cdot}10^{19}$ cm^{-2}, and the density in the hard X-ray source of length ∼65 Mm has to be below $\sim 10^{10}$ cm^{-3}. Using these limits, the instantaneous number of electrons above 20 keV, N_{inst}, in the hard X-ray producing source is $4{\cdot}10^{32} << N_{inst} < 1{\cdot}10^{35}$. Using the ballistic transit time in radial direction (∼0.8 s) as a rough estimate for the time electrons spend in the hard X-ray source and a total duration of ∼20 s of the hard X-ray emission, a total of $1{\cdot}10^{34} << N_{total} < 3{\cdot}10^{36}$ electrons above 20 keV are needed to produce the observed hard X-ray emission in the thin target approximation. For longer transit times (e.g. propagation at pitch angles different from zero), the column density increases and the number of needed electrons can be smaller. For comparison, we also mention here that in the thick target approximation, N_{total} becomes $9{\cdot}10^{33}$ electrons above 20 keV.

To derive the number of escaping electrons from the in-situ WIND observations is difficult because no information on the angular extent of the electron event exists. Furthermore, the observed electron flux is only a lower limit, because WIND could miss the peak flux and only observe at the flank of the event. The derived values here therefore are only order of magnitude estimates. Assuming a cone of 60°, the number of escaping > 20 keV electrons, $N_{in-situ}$, becomes $3{\cdot}10^{33}$. This is a typical value for an average-sized event (e.g. Lin & Hudson 1971), but less by at least an order of magnitude than what is needed to produce the observed hard X-ray emission in the thin target approximation.

3. Discussion & Summary

This paper presents the first detection and imaging of a purely coronal hard X-ray source that is associated with escaping electron beams producing radio type III bursts. Several of the observed characteristics suggest that thin target X-ray emissions from the escaping electrons are seen:

- The onset of the hard X-ray emissions are temporally correlated with type III radio bursts. The hard X-ray duration is longer by about a factor of three suggesting that only the front of the electron beam produces radio waves.
- Hard X-ray imaging reveals a coronal source elongated in the radial direction with a source length similar to typical coronal density scale heights.

- The hard X-ray photon spectral index is larger by ∼1 than the in-situ observed electron spectrum.

The only unclear point in the thin target interpretation is that the order of magnitude estimate of the number of escaping electrons is at least an order of magnitude too low to explain the intensity of the detected hard X-ray emission. However, this estimate is derived from a single-spacecraft measurement and it is therefore highly uncertain. Because the flare site is far away from the footpoint of the nominal Parker spiral, it could be possible that WIND measurements are not taken at the location of maximum flux, but at the flank of the event where the electron flux is expected to be lower. The event presented here is only an average-sized event with the largest detected events having fluxes up to ∼50 times larger. It could therefore be possible that the derived number of escaping electrons is significantly underestimating the actual value.

A smaller number of electrons to produce the observed hard X-ray emission would be needed if pitch angle scattering increases the time the electron beam spent in the hard X-ray source (in the estimates used above, ballistic 'scatter-free' transport is assumed). Additionally, the hard X-ray intensity might also be increased if collisional losses in the hard X-ray sources might become energetically important, at least for electrons at lower energies. The emission mechanism would than be a partially thick scenario and the number of electrons would be reduced. However, collisions would also change the electron spectral shape, at least at lower energies.

The influence of the different uncertainties are very difficult to estimate. Nevertheless, we tried to estimate their maximal influence: a) Taking observations at the flank of the event could underestimate the number of electrons by maybe up to a factor of 10. b) The angular extent of the electron event could be larger by a factor of 2. c) Assuming an average pitch angle of the hard X-ray producing electron different from zero might reduce the number of needed electrons by a factor of 2. d) A partially thick scenario that does not change the spectrum more than the observed uncertainties of the spectral results could make the number of needed electrons smaller by a factor of 2. Considering these factors, the number of escaping electrons could be consistent with the thin target scenario. However, the available data is not conclusive.

It should also be mentioned, that the observations presented here cannot exclude the interpretation that the observed hard X-ray emission is produced by downwards-moving electrons instead of outwards-moving ones. In this scenario, the acceleration site is above the observed hard X-ray source and both up and downwards moving electron beams are created. The observed elongated partially disk-occulted hard X-ray source might still be produced in the thin approximation. However, to make the thin target interpretation work,

the up and downwards moving electron beams would need the same spectral shape.

Favorable conditions made the detection of coronal hard X-ray emissions associated with radio type III bursts and an impulsive electron event possible: 1) the main flare emission was disk-occulted, but 2) magnetic field lines from the flare site were nevertheless well connected with the WIND spacecraft near 1 AU, and 3) the radio emission was able to escape to Earth. These conditions are only rarely fulfilled making it generally difficult for RHESSI to observe hard X-rays from escaping beams with simultaneous in-situ observations from a near Earth orbiting spacecraft. However, a systematic search in the RHESSI and Wind/3dp data set is in preparation to investigate this in detail. Including multi-point STEREO observations will greatly help the search for more events, as condition 2) and 3) can be relaxed. Although faint (i.e. same order of magnitude as the RHESSI background emission), many hard X-ray observations of escaping electron beams without simultaneous observations of impulsive electron events should exist in the RHESSI data base. It is difficult to find these events because any additional X-ray emissions will hide the emission related to type III bursts. Nevertheless, a systematic search is planned including radio imaging observations by the Nancay Radio Heliograph. Future multi-spacecraft observations in the inner hemisphere by the Solar Orbiter and Sentinels mission will frequently provide simultaneous hard X-ray and in-situ observations with up to a factor of $\sim$15 higher X-ray sensitivity and will revolutionize our understanding of electron acceleration and transport.

The work was supported through NASA contract NAS 5-98033 for RHESSI, NASA L-WS grant NNX06AC18G for scientific activities with GBSRBS, and Heliophysics GI award NNX07AH76G. STEREO/WAVES data analysis at UCB is support by NASA grant N-NX07AD91G to the University of California. Hinode is a Japanese mission developed and launched by ISAS/JAXA, with NAOJ as domestic partner and NASA and STFC (UK) as international partners. It is operated by these agencies in co-operation with ESA and NSC (Norway). We would like to thank the Hinode team for making their data available online.

REFERENCES

Aurass, H., Klein, K.-L., & Martens, P. C. H. 1994, Sol. Phys., 155, 203

Battaglia, M., & Benz, A. O. 2006, A&A, 456, 751

Bougeret, J.-L. et al., 1995, Space Sci. Rev., 71, 231

Bougeret, J.-L. et al., 2008, Space Sci. Rev., in press

Bastian, T. S., Benz, A. O., & Gary, D. E. 1998, ARA&A, 36, 131

Brown, J. C., 1971, Sol. Phys., 18, 489

Dröge, W. 1995, International Cosmic Ray Conference, 4, 191

Emslie, A. G. 1978, ApJ, 224, 241

Frost, K. J., & Dennis, B. R. 1971, ApJ, 165, 655

Golub, L., Austin, G., Bookbinder, J., Caldwell, D., Cheimets, P., & Cirtain, J., . 2007, Solar Physics, 243, 63

Haggerty, D. K. and Roelof, E. C., 2002, ApJ, 579, 841

Hannah, I.G., Christe, S., Krucker, S., Hurford, G.J., Hudson, H.S., Lin, R.P., 2008a, Astronomy & Astrophysics, in press

Hudson, H. S. 1978, ApJ, 224, 235

Hudson, H. S., Fletcher, L, Kahn, J.I., & Kosugi, T. 2004, D.E. Gary and C.U. Keller (eds.), Kluwer, Solar And Space Weather Radiophysics, 153-178

Hudson, H. S., Bougeret, J.-L., & Burkepile, J. 2006, Space Science Reviews, 123, 13

Hurford, G. J., et al. 2002, Sol. Phys., 210, 61

Kane, S. R., McTiernan, J., Loran, J., Fenimore, E. E., Klebesadel, R. W., & Laros, J. G. 1992, ApJ, 390, 687

Klein, K.-L., Krucker, S., & Lointier, G. 2008, Astronomy & Astrophysics, submitted

Kosugi, T., et al. 2007, Sol. Phys., 243, 3

Krucker, S., Larson, D. E., and Lin, R. P., & Thompson, B. J., 1999, ApJ, 519, 864

Krucker, S., Kontar, E. P., Christe, S., & Lin, R. P. 2007a, ApJ, 663, L109

Krucker, S., White, S. M., & Lin, R. P. 2007b, ApJ, 669, L49

Krucker, S., Hannah, I. G., & Lin, R. P. 2007c, ApJ, 671, L193

Krucker, S., & Lin, R. P. 2008, ApJ, 673, 1181

Krucker, S., Hurford, G. J., MacKinnon, A. L., Shih, A. Y. ,& Lin, R. P. 2008, ApJ, in press

Lin, R. P., & Hudson, H. S. 1971, Sol. Phys., 17, 412

Lin, R. P., 1985, Sol. Phys., 100, 537

Lin, R. P. et al., 1995, Space Sci. Rev., 71, 125

Lin, R. P., et al. 2002, Sol. Phys., 210, 3

Lintunen, J. and Vainio, R., 2004, A&A, 420, 343

Masuda, S., Kosugi, T., Hara, H., Tsuneta, S., & Ogawara, Y. 1994, Nature, 371, 495

Nitta, N.V, Mason, G.M., Wiedenbeck, M.E., Cohen, C.M.S., Krucker, S., Hannah, I.G., Masumi Shimojo, M., & Shibata, K. 2008 ApJ, in press

Pick, M., Mason, G. M., Wang, Y.-M., Tan, C., & Wang, L. 2006, ApJ, 648, 1247

Reiner, M. 2001, Space Science Reviews, 97, 129

Saint-Hilaire, P., Krucker, S., & Lin, R.P.. 2008, ApJ, submitted

Saiz, A., Evenson, P., Ruffolo, D., and Bieber, J. W., 2005, ApJ, 626, 1131

Somov, B., Kosugi, T., Masuda, S., Sakao, T., & Bogachev, S. A. 2004, 35th COSPAR Scientific Assembly, 35, 14

Sui, L., & Holman, G. D. 2003, ApJ, 596, L251

Tomczak, M. 2001, A&A, 366, 294

Wang, Y.-M., Pick, M., & Mason, G. M. 2006, ApJ, 639, 495

Wibberenz, G., & Cane, H. V. 2006, ApJ, 650, 1199

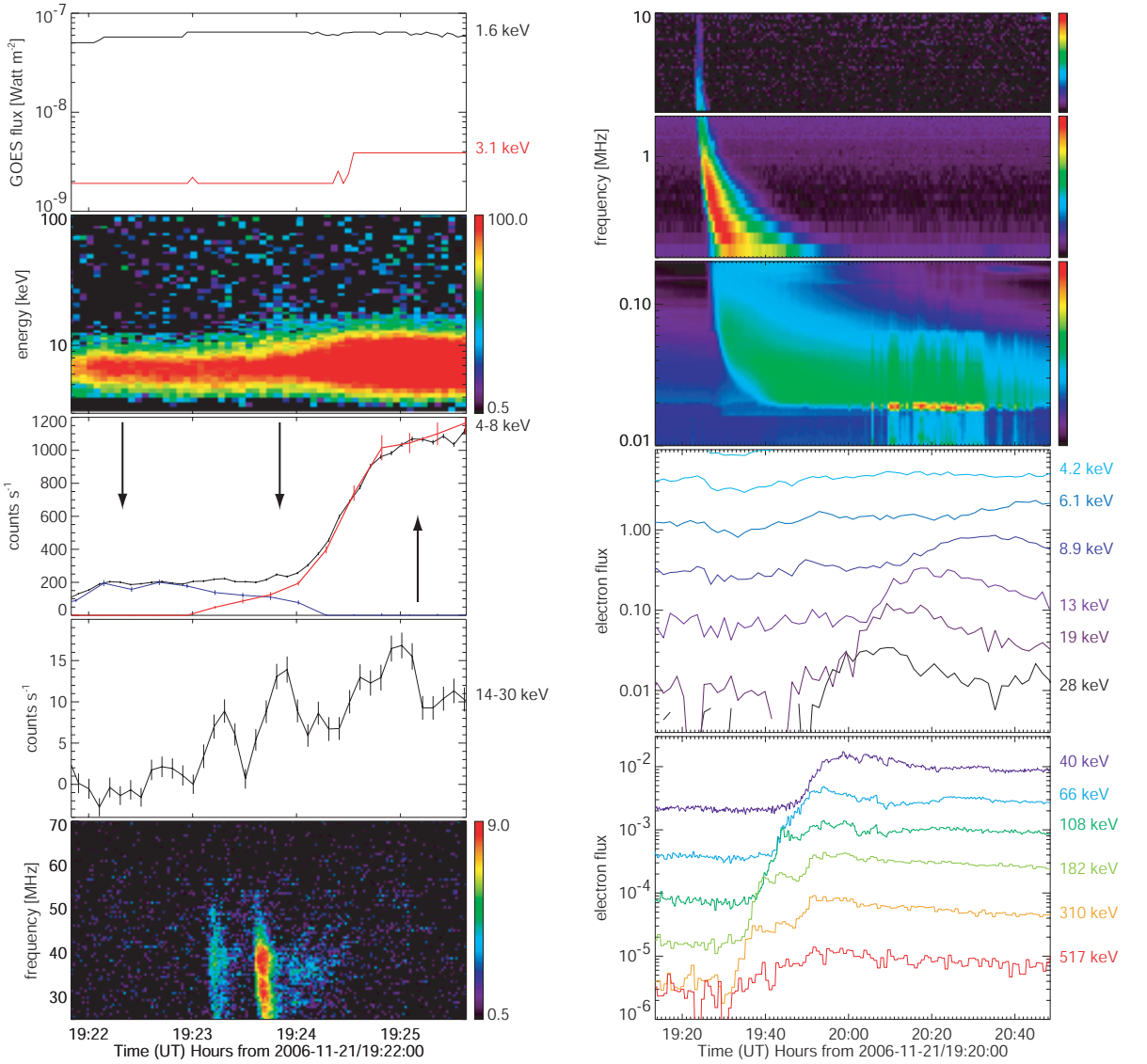

Fig. 1.— X-ray, radio, and electron flux time profiles of the November 21, 2006 event. (left) The top four panels show X-ray observations from GOES (top) and RHESSI at different energies as indicated. The 4-8 keV time profiles in the middle panel show the total count rate in black and the time profiles of the individual sources are given in blue and red (cf. Figure 2). The bottom panel shows radio spectrogram from GBSRBS. (right) The top three panels give radio type III burst observations from STEREO/WAVES and WIND/WAVES, respectively, and the two panels below show electron fluxes observed by WIND/3dp near 1 AU. The arrows give the times of the images shown in Figure 2.

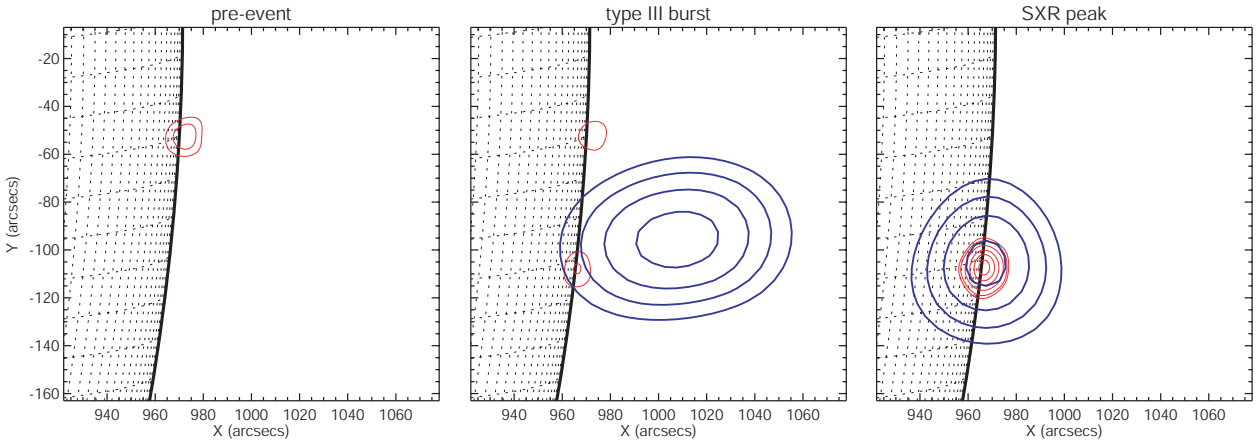

Fig. 2.— RHESSI X-ray imaging before (left, 19:22:20 UT), during (middle, 19:23:46 UT), and after (right, 19:25:05 UT) the radio type III bursts. Thermal emission (4-8 keV) is shown in red contours (levels are 5, 10, 30, 50, 70, 90% of the peak intensity at 19:25:05 UT) with 10″ FWHM resolution, and the 14-30 keV emission is given in blue (levels are 65, 75, 85, and 95%) with a resolution of 60″. For the temporal evolution of the different sources compare with time profiles shown in Figure 1.

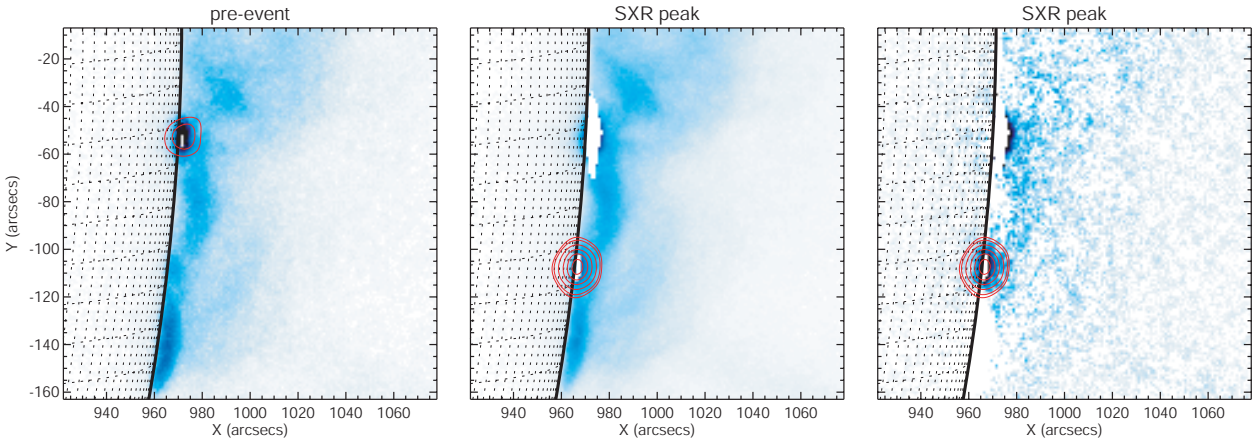

Fig. 3.— RHESSI and HINODE X-ray imaging: XRT images are only available ∼2 minutes before the type III burst (19:21:47 UT, left) and ∼3 minutes after (19:26:48 UT, center). The difference image is shown to the right. The shown images are taken with the 'medium Be' filter. Dark is enhanced emission and saturated pixel are shown in white. (Note that the exposure time is longer for the later image and the larger number of saturated pixels therefore does not necessarily indicated enhanced emission). The RHESSI 4-8 keV contours are the same in Figure 2. Although there is a weak enhancement observed connecting the two main thermal sources, no X-ray jet is observed. The interpretation of the HINODE soft X-ray observations is unclear.

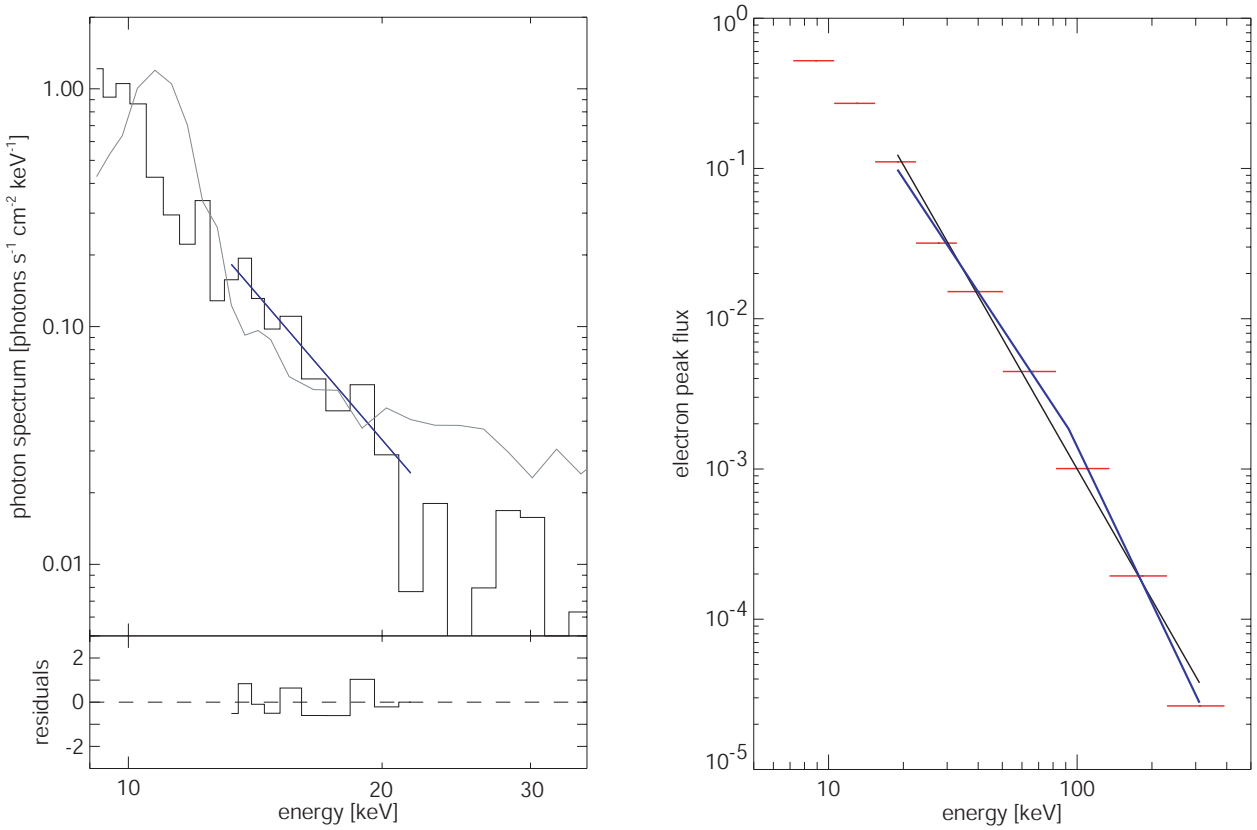

Fig. 4.— (left) The background-subtraced hard X-ray spectrum averaged over 12 s around 09:50:50 UT is shown in black. The observations are by a fitted power law function in the energy range between 14-25 keV (blue curve, power law index is $\gamma = 4.1 \pm 0.4$). The gray line represents the background emission, and the panel below shows the normalized residuals of the fit. (right) Electron peak flux spectrum observed at 1 AU by WIND/3dp. Two fits to the data are shown: In black, a power law fit to the data above 20 keV with a slope of $\delta = 2.9 \pm 0.3$, and in blue, a broken power law fit with $\delta = 2.5 \pm 0.4$ below $\sim$90 keV, and $\delta = 3.5 \pm 0.4$ above.